Microgravity Science and Technology

Complementary techniques for the accelerometric environment characterization of thermodiffusion experiments on the ISS

--Manuscript Draft--

Manuscript Number:	
Full Title:	Complementary techniques for the accelerometric environment characterization of thermodiffusion experiments on the ISS
Article Type:	TC_Mr_Microgravity
Keywords:	IVIDIL; DCMIX; SEN technique; RMS warning map; nonlinearities of the ISS acceleration signals; ISS vibrational environment
Corresponding Author:	Fina Gavaldà, PhD Universitat Rovira i Virgili Tarragona, Tarragona SPAIN
Corresponding Author Secondary Information:	
Corresponding Author's Institution:	Universitat Rovira i Virgili
Corresponding Author's Secondary Institution:	
Order of Authors:	Diana Dubert, PhD
	Marc Marín-Genescà, PhD
	Maria José Simón, Engineer
	Fina Gavaldà, PhD
	Xavier Ruiz, PhD
First Author:	Diana Dubert, PhD
First Author Secondary Information:	
Order of Authors Secondary Information:	
Funding Information:	Ministerio de Ciencia, Innovación y Universidades, Gobierno de España, and the European Regional Development Fund (FEDER) (ESP2017-83544-C3-3-P) — Professor Xavier Ruiz
	Universitat Rovira i Virgili (2018PFR-URV-B2-73) — Professor Xavier Ruiz
Abstract:	The accelerometric environment of IVIDIL and DCMIX experiments was successively monitored not only to identify the main disturbances that could affect the experiments but as well to ensure the correct interpretation of the experimental results. To do so, the conventional techniques used by NASA have been complemented by new tools developed and adapted to help the surveillance of the runs. A summary of these main new techniques is presented further. To show the potentiality of all these techniques, moderate and strong disturbance episodes such as berthings, dockings and reboostings were analyzed by using acceleration signals that come from three different sensors located in the US Lab. Destiny, Columbus and JEM/Kibo modules, respectively. The first technique proposed is based on the Shannon entropy concept in both time (TEN) and frequency (SEN) domains. It has been found, that SEN technique is a fast and easy tool to detect the different disturbances registered throughout the experiments. The second technique suggested by the authors is based on the RMS values integrated over each one of the one-third octave frequency bands and is called RMS warning map. It is a visual tool which was demonstrated to be very efficient in detecting the range of the frequencies that surpasses the ISS limits requirements, especially when a sudden disturbance occurs. Finally, in order to identify nonlinearities in the frequency domain within a signal, bispectrum and trispectrum functions have

	been applied. Quadratic and cubic phase couplings have been detected with these techniques only between high frequencies and especially for the signal from JEM/Kibo module.

Complementary techniques for the accelerometric environment characterization of thermodiffusion experiments on the ISS

D. Dubert[a], M. Marín-Genescà[b], M.J. Simón[b], Jna. Gavaldà[a*], X. Ruiz[a,c]

[a] Universitat Rovira i Virgili, Departament Química Física i Inorgànica. Tarragona, Spain.
[b] Universitat Rovira i Virgili, Departament d'Enginyeria Mecànica, Tarragona. Spain.
[c] Institut d'Estudis Espacials de Catalunya, IEEC. Barcelona. Spain.
*Corresponding author: fina.gavalda@urv.cat; Phone: +34 977559518
ORCID of corresponding author: 0000-0001-7881-4192

Abstract

The accelerometric environment of IVIDIL and DCMIX experiments was successively monitored not only to identify the main disturbances that could affect the experiments but as well to ensure the correct interpretation of the experimental results. To do so, the conventional techniques used by NASA have been complemented by new tools developed and adapted to help the surveillance of the runs. A summary of these main new techniques is presented further. To show the potentiality of all these techniques, moderate and strong disturbance episodes such as berthings, dockings and reboostings were analyzed by using acceleration signals that come from three different sensors located in the US Lab. Destiny, Columbus and JEM/Kibo modules, respectively. The first technique proposed is based on the Shannon entropy concept in both time (TEN) and frequency (SEN) domains. It has been found, that SEN technique is a fast and easy tool to detect the different disturbances registered throughout the experiments. The second technique suggested by the authors is based on the RMS values integrated over each one of the one-third octave frequency bands and is called RMS warning map. It is a visual tool which was demonstrated to be very efficient in detecting the range of the frequencies that surpasses the ISS limits requirements, especially when a sudden disturbance occurs. Finally, in order to identify nonlinearities in the frequency domain within a signal, bispectrum and trispectrum functions have been applied. Quadratic and cubic phase couplings have been detected with these techniques only between high frequencies and especially for the signal from JEM/Kibo module.

Keywords: IVIDIL; DCMIX; SEN technique; RMS warning map; nonlinearities of the ISS acceleration signals; ISS vibrational environment

Acknowledgements

The present work has been supported by the Spanish Ministerio de Ciencia, Innovación y Universidades and the European Regional Development Fund (FEDER) (grant number: ESP2017-83544-C3-3-P) and by the Universitat Rovira i Virgili (URV) (grant number 2018PFR-URV-B2-73).

1.- Introduction

As a result of NASA's efforts, and in particular the PIMS NASA team, the accelerometric environment of the ISS is public, digital signals of acceleration coming from SAMS (Space Acceleration Measurement System)– and MAMS (Migrogravity Acceleration Measurement System) - sensors, can be downloaded and examined without restrictions (PIMS website: PIMS 2018). In addition, PIMS NASA website offers a first immediate data analysis based on standard digital processing techniques (see Table 1) (Rogers et al. 1997; Hrovat 2004, b; Kelly 2004; McPherson et al. 2015). Using these techniques different episodes covering the Station's orientation maneuvers to the internal mechanical equipment are examined in detail. All results are compiled in a Handbook that can also be consulted freely on the website (PIMS website: PIMS 2018; McPherson et al. 2015).
But, complementing this global strategy there is a more specific approach which only focuses on the surveillance of a single experiment to characterize the different runs associated with it. This point of view is suitable when the experiments are related to the diffusion-thermodiffusion phenomenon because thermal and solutal convection can mask their coefficients evaluation on Earth laboratories. A space platform, such as the ISS (International Space Station), is thus more adequate. In these cases, due to the own nature of the physical processes, experiments take a long time and it is particularly interesting to know the peculiarities of the accelerometric environment as a potential source of experimental errors in the quantitative determination of these coefficients. To do this, additional signal processing techniques (see Table 1) have been implemented by the authors.
In this context, the first experiment monitored was the IVIDIL (Influence of VIbrations on DIffusion in Liquids, Shevtsova 2010) conducted during the period 2009-2010 and aiming to examine the vibroconvective effects in the quantitative determination of the diffusion and thermodiffusion coefficients of water-isopropanol mixtures. The most important consequence of the vibratory environment characterization was to detect nonlinearities in the acceleration signals (Sáez et al. 2013, 2014a, 2014b, 2014c, 2015). The second monitored diffusion-thermodiffusion experiment was the DCMIX (Diffusion and Thermodiffusion Coefficients Measurements in Ternary Mixtures) series, started in 2011 (DCMIX1) and continued till present (DCMIX4). The aim of all these experiments was to accurately measure pure diffusion, thermodiffusion and Soret coefficients of relevant ternary liquid systems. In the first campaign, DCMIX1 (2011-2012), the mixture selected was representative of a simplified model of the oil reservoirs composition (Mialdun et al 2015). This selection responds to the fact that in oil reservoirs, the thermodiffusive effect plays an important role due to the presence of geothermal gradients. The second campaign, DCMIX2 (2013-2014), focused on the toluene-methanol-ciclohexane ternary system because it was detected a broad miscibility region in it which allows to study how transport coefficients diverge when approaching this region (Shevtsova et al 2014). In the third campaign, DCMIX3 (2016), water-ethanol-triethylene glycol mixtures was investigated due to its variable Soret coefficient sign (positive and negative) that had already been detected for certain binary subsystems (Triller et al 2018). Finally, the fourth campaign, DCMIX4 (2018 -2019) will seek to

expand the above characterizations to a wide range of systems such as the ternary polymer system (polystyrene-toluene-hexane) and the ternary nanofluid ones (tetralin-toluene-fullerene) with applications ranging from photovoltaics to biotechnology.
To monitor the accelerometric behavior of all these experiments, SAMS data covering the whole vibratory range (0.01-300 Hz) have been examined (Jurado et al; Ollé et al. 2017; Dubert et al 2018). A special attention has been paid for the active periods (dockings/undockings, berthings/deberthings, reboostings) detected during the experiments due to their possible influence in the evaluation of the thermodiffusion coefficients. One of the conclusions drawn from the above vibratory characterization is that the acceleration signal varies in time and also depends on the NASA's module in which is measured. This means that the information more adjusted to the interest of the experimentalists can be considered minute by minute and coming from the sensor located as close as possible to the corresponding experiment, the onsite sensor. For example, in IVIDIL and DCMIX experiments, the suitable SAMS sensor was located inside the Glovebox (Jurado et al; Ollé et al. 2017).
As mentioned before, some complementary procedures have progressively been developed and introduced by the authors, in the field of characterization of the acceleration signals. The aim of the present paper is thus to compile, revise and complete the most representative procedures developed to help thermodiffusion experimentalists. Examples to illustrate the general potentialities of these techniques are based on real acceleration signals downloaded from PIMS NASA website (PIMS website: PIMS 2018) coming from three different SAMS sensors located in a) the US Lab., Destiny (121f03), b) the Columbus (121f02) and c) the JEM/Kibo modules (121f05), respectively. In particular, three different kind of disturbances which potentially could affect the microgravity quality of the ISS environment were selected (Marín-Genescà et al 2018). The first one was an unmanned HTV5- Kounotori berthing episode occurred in August 2015. In this case the ISS's Canadarm 2 robotic arm grappled and fastened the craft to the ISS's Common Berthing Mechanism in the Nadir port of Node 2, Harmony. The second disturbance was an unmanned Progress MS-02 (Mission 63P) cargo docking episode taking place in April 2016 to resupply the ISS. This cargo spacecraft used the aft port of the Zvezda module to be attached. The third selected disturbance was a reboosting episode completed in November 2016 by using the Zvezda Service Module main engines. Remark that, in all cases the acceleration components used here in the calculations refer to the Space Station Absolute coordinate system, SSA.

2.- Complementary Digital Signal Techniques

The first complementary technique is based on the entropy concept (EN) acting as single scalar summarizing the changes in time and/or frequency distributions. The second one is the RMS warning map, serving as a visual global indicator of the microgravity quality all along an experiment. Finally, the third technique is related with a particular aspect of the spectral nonlinearities detected in the distribution of the signal's energy.

2.1.- Entropy

For the first time Clausius introduced the concept of entropy in the middle of the 18^{th} century as a precise way of expressing the second law of thermodynamics. Later, Boltzman incorporated a statistical basis to this concept identifying it with the degree of disorder of a given system (the entropy of a system increases if it tends to a disordered state). After this generic identification, the entropy and its variants have become a popular concept used in a variety of applications. For instance, the growth of telecommunications in the early twentieth century led several researchers to measure the amount of information contained in a signal in terms of Shannon entropy (Shannon 1948). Based on the above concept, the present work focuses on summarizing in a single scalar the time and frequency distribution changes associated to any acceleration signal.

2.1.1.- Time Entropy

From a mathematical point of view, the time entropy of a discrete signal of acceleration, is defined as

$$TEN = -\frac{1}{\log(N)} \sum_i p_i \cdot \log(p_i) \qquad (1)$$

where N is the number of discrete probabilities p_i used in the sum Σ_i (Shannon 1948). Alike all entropies, this magnitude seeks to quantify the degree of order/disorder of the values contained in the signal, however, regardless of its valuable information, it is very generic and at the moment does not bring any relevant additional information to the signal characteristics. To solve this deficiency a relative entropy, TEN_r, has been introduced which compares the entropy of the signal with the entropy corresponding to a discrete Gaussian distribution fitting the signal and with the same number of bins N. In this way, the Gaussian character of any signal of acceleration relates to

$$\mathrm{TEN}_r = 100 \cdot \frac{|TEN - TEN_{Gauss}|}{TEN_{Gauss}} \qquad (2)$$

The reason to consider the above comparison, specifically the probability density function of the Gaussian distribution, comes from its enormous relevance in statistics and probability theories in terms of real-valued random variables whose distributions are known. Moreover, it is important to remember that many results can be derived analytically when the relevant variables are normally distributed.
Such an example is Figure 1.a showing the minute by minute evolution of the relative time entropy, TEN_r of the selected HTV5 berthing episode coming from three different ISS modules (USlab, Columbus and Kibo). Due to the characteristics of this manoeuver, calculations are restricted here to the direction of the disturbance (Z_A). A total time of eight hours over records of one minute each has been considered in order to examine the significant changes in signal's TEN. To complement the information, the minute by

minute skewness and kurtosis values have also been plotted simultaneously [Figs 1.b and 1.c]. Both parameters clarify even more the shape of the distribution associated to the signal, the skewness its asymmetry and the kurtosis its tails. Results corresponding to the USLab show small continuous variations of the relative TEN, near zero, indicating that the acceleration signal may be a consequence of the sum of many independent physical processes (Central Limit Theorem). Columbus and JEM/Kibo results report abrupt but significant deviations. These short episodes could be related to the first berthing contact or other important mission events such as the removal of the Exposed Pallet from the HTV5 Unpressurized Logistics Carrier and its transfer to the JEM/Kibo's Exposed Facility or even the crew ingress to the Pressurized Logistics Carrier, PLC for the subsequent cargo transfer from PLC to the Station. The reason of the different modules sensitivity is likely a consequence of the relative different module orientation to the berthing direction.

2.1.2.- Spectral entropy

The spectral entropy, SEN, associated to any acceleration signal is defined based on the normalized power spectral density, PSD, of that signal as follows

$$SEN = -\frac{1}{\log(N)} \sum_f [PSD_f \cdot \log(PSD_f)] \qquad (3)$$

If the whole spectral contents of the signal is considered, N is the number of discrete frequency bins used in the sum Σ_f and the sub-index f goes to its cut-off value. If, on the contrary, the signal has been previously filtered restricting its spectral contents below a certain frequency limit the sub-index f then indicates the values till the frequency limit considered in the filtering. Remark that, the normalization of the power spectrum is not a suitable indicator for detecting signal's amplitude variations. Thus, the spectral entropy is only related to the frequency distribution summarizing in a single scalar the degree of dispersion of its spectral energy. A high value of entropy, roughly unity, indicates that the energy spectrum of the signal is distributed all along the frequency range. A low value, of the order of zero, means that the energy is concentrated in a group of frequency bands. Therefore, the changes in the spectral entropy can be used as a robust tool to identify possible signal's disturbances, considering that these disturbances come accompanied by a significant change in the spectral distribution. This is justified, for instance, for the fact that the spectral entropy was found to be an excellent detector of spikes if the frequency domain is examined due to the new low frequencies appearance (Ollé et al 2017).

In an attempt to explain clearer the SEN behavior as a function of changes in the spectral distribution, the corresponding minute by minute spectrogram has systematically been presented in such a way that one horizontal line of the spectrogram is equivalent to a PSD of one-minute acceleration signal corresponding to one point of the SEN line located at the same horizontal level (See Fig.2). With respect to this, the spectrograms are only considered for comparison to the SEN, avoiding any additional consideration derived

from the Heisenberg-Gabor inequality in time and frequency resolution. Due to the possibility of election of a frequency threshold, the calculation of SEN also enables to separate contributions from different frequency ranges in order to observe specific alterations inside these ranges. This feature is interesting in case of comparisons between the full frequency contents of an acceleration signal and a reduced range containing, for instance, the low frequency part of it. In the present work both SEN_{all} and SEN_{20} have been systematically considered. In the first case, the whole frequency range was used, while in the second one frequencies below 20 Hz were selected for calculations.
To do so, instead of the classical filtering based on Fourier analysis, a denoising technique based on the Discrete Wavelet Transform (DWT) has been applied. Based on a mother wavelet function and on the Fast Wavelet Transform algorithm the calculation of the different coefficients of the discrete transform was made by the use of a dyadic filter bank. This bank decomposes the signal's broadband into a collection of successively band limited components by repeatedly dividing the frequency range. However, for the wavelet reconstruction of the signal only the low-frequency output of the previous level is newly decomposed into two adjacent high and low frequency sub-bands by a high and low-pass filter pair. Each one of these two output sub-bands is approximately half the bandwidth of the input to that level. The successive elimination of the high-frequency sub-bands works considerably better in the reconstruction of the signal compared to the classical filtering procedures, especially in the case of additive Gaussian white noise spreading in all frequencies (Jurado et al 2016). In the present case, sym8 Symlet was used as mother wavelet function with a decomposition level fixed at four, implying that the signal was filtered at frequencies roughly lower than 20 Hz.
Figure 2 shows the SEN evolution (right side) and the corresponding spectrograms (left side) of the Progress SM-02 (Mission 63P) docking episode. Due to the fact that this spacecraft used the aft port of Zvezda module, calculations were restricted to three acceleration signals in the direction of the disturbance (X_A). All signals were studied for a total time of eight hours over records of one minute each, including the docking episode in the middle (4h). Given the fact that the coupling between the spacecraft and the Station is a long lasting procedure requiring maneuvers that involves both the spacecraft and ISS respectively, before and after the attachment, the SEN information is very spiked in all cases. In case of Columbus and JEM/Kibo modules (see Figs. 2b and 2c) the large variation of the spectral contents below roughly 1 Hz in the spectrogram perfectly explains these strong oscillations. In the US Lab Destiny, and probably due to the position of the module along the direction of the perturbation, a decrease of SEN oscillation is detected (see Fig. 2). When high frequencies dominate the spectrum, different mean values of SEN could be observed, for the two frequency ranges selected (see Figs.2a and 2c). This might be due to the different spectral contents between the raw (all frequencies range) and of the denoised signals (frequencies lower than 20 Hz).
Regarding Fig. 3 the spectrograms and the corresponding SEN evolution were plotted for Zvezda reboosting episode. As mentioned before, the calculations are restricted to three acceleration signals in the direction of the disturbance (X_A). Spectrogram and SEN, have also been constructed for a total time of eight hours over records of one minute, including the reboosting period centered at 4h. Since the reboosting maneuver introduces short

changes in the low frequency range, SEN can clearly detect them. In present case reboosting period lasted approximately 140 seconds, therefore a set of sharp peaks in the middle part of SEN_{20} plots perfectly correlates with the disturbance.

Summarizing, SEN is an optimal complementary tool to detect sharp and time concentrated disturbances (RMS peaks (Triller et al. 2018) and reboostings). Though, for time extended disturbances (docking, berthings, undockings or deberthings) this information is insufficient to associate the SEN changes with the variations provoked by the disturbance itself.

2.2.- Warning maps

Based on the PSD evaluation and using the Parseval theorem, the one-minute RMS level associated to any acceleration signal a_j, integrated over each one of the one-third octave band, is calculated using Rogers et al 1997 and Hrovat 2004 expression

$$RMS(a_j) = \sqrt{\sum_{i=flow_j}^{i=fhigh_j} [PSD(a_i)] \cdot \Delta f} \qquad (4)$$

where Δf represents the frequency resolution in the evaluation of the PSD and $flow_j, fhigh_j$ are the minimum and maximum frequency values in the j frequency band calculated by the expressions:

$$flow_j = 0.1 \cdot 2^{\frac{j-1}{3}} \cdot 2^{-\frac{1}{6}} \;\; ; fhigh_j = 0.1 \cdot 2^{\frac{j-1}{3}} \cdot 2^{\frac{1}{6}} \qquad (5)$$

NASA's International Space Station vibratory limit requirements based on Root Mean Square (RMS) are defined by Rogers et al 1997 and Hrovat 2004

$$0.01 \leq f \leq 0.1\,Hz,\;\; RMS \leq 1.8\;\; \mu g \qquad (6)$$
$$0.1 \leq f \leq 100\,Hz,\qquad RMS\;\leq 18 \cdot f\;\; \mu g \qquad (7)$$
$$100 \leq f \leq 300\,Hz,\;\; RMS\;\; \leq 1800\;\; \mu g \qquad (8)$$

Assuming that the values of the $RMS(a_j)$ in any band are lower than the corresponding threshold (1.8 µg, 18f µg and 1800 µg) the environment can be considered in microgravity mode. Under these conditions it can be expected that the accelerometric environment does not influence the experimental results. A quick visual way to display if the vibratory limits have been surpassed or not, along the experiment, is given by the RMS warning map technique which thus, can be important for the experimentalists. In this way, given a particular acceleration signal, the comparison between the standard NASA's ISS vibratory limit requirements and its corresponding one-minute RMS levels is the basis of each horizontal line of the warning map. Points in the RMS warning map represent each ISS vibratory limits exceeded. Remark that, the present comparison includes only the

excess and not the amount of excess respect to the vibratory limits, therefore the warning map is only qualitative. Despite of its qualitative character it enables an easy identification of the problematic frequency bands, at a specific time, that outdo the ISS limit requirements.
To illustrate the above information Fig. 4 plots, on one side, the RMS warning map (Fig.4 b) corresponding to Progress MS-02 (63P Mission) docking outset and on the other, the ISS limit requirements as RMS values at minute 240, as comparison (Fig. 4a). The calculations were restricted to the three acceleration signals considered before, in the direction of the disturbance, X_A. It can be noticed that RMS values are close to the limit curve, crossing it only at frequency ranges lower than 1 Hz in all modules. The presence of these low/structural frequencies are practically constant all along the eight hours considered and mainly visible in the Columbus and JEM/Kibo modules. This reinforces the fact that docking procedures are very noisy and long lasting disturbances. The technique can be as well, applied for other disturbances such as reboosting performed by Progress MS-02 (63P Mission). Fig. 5b then, shows the corresponding warning maps coinciding with the reboosting period (at 4 h) which is perfectly detected at frequencies lower than 1 Hz. In addition, the microgravity mode conditions are accomplished for frequencies above 5 Hz in all cases except the US Lab (see Figs. 5a1 and 5b1) where a frequency close to 100 Hz, that outdo the ISS limits, is detected. This high value might be related to the life support machinery, the Common Cabin Air Assembly, which contains a rigid axis spinning at approximately 6000 rpm. The values of the RMS during one minute of the reboosting period is as well represented in Fig. 5a.
Summarizing, the RMS warning map is a proper tool to detect the increase of the PSD intensities at specific range of frequencies when a disturbance takes place.

2.3 Nonlinearities in the frequency domain

As it is well-known, nonlinearities in time series can be detected by using specific statistical tools such as, the surrogated data testing. If the result is positive, a robust set of techniques can help in the characterization of the mechanical system associated (Kantz and Schreiber 2005). However, if the objective of the study is focused to investigate the existence of nonlinearities affecting the energy distribution of a signal, Higher Order Statistical Analyses, HOSA, techniques are different way to solve the problem (Sáez et al. 2013). In fact, in the field of mechanical vibrations a lot of diagnosed faults are based on the application of these techniques to the acceleration signals gathered from aging rotating machinery (nonlinear systems such as old motor bearings or rotor misalignments). In aerospace, on the contrary, only a few works have introduced these techniques to investigate this kind of nonlinearities. This is a surprising situation because malfunctions in motorized experiments, if any, are not easy to be removed in space platforms and, in the worst case, could change the nominal conditions of the experiment confusing the experimentalist and generating doubtful results. Concerning the energy distribution of a signal, it is important to remember that the power spectral density (second order spectrum) provides very useful, but incomplete, information. This is because it suppresses any phase relationship, is not sensitive to phase changes and cannot be used for the detection of phase couplings. The only technique suited to do this is HOSA.

The first magnitude used in these kind of analyses is the bispectrum (third order spectrum). On the grounds that, this magnitude is related to the skewness of the signal, bispectrum can detect asymmetric nonlinearities. Mathematically is defined as,

$$|S_k(f_1, f_2)| = |X(f_1) \cdot X(f_2) \cdot X^*(f_1 + f_2) \qquad (9)$$

$$\angle S_k(f_1, f_2) = \theta(f_1) + \theta(f_2) - \theta(f_1 + f_2) \qquad (10)$$

where $\mathrm{X}(f_i)$ denotes de Fourier Transform of the acceleration considered at the frequency f_i, X^* its complex conjugate and $\theta(f_i)$ the phase of the Fourier Transform X at a frequency f_i. The method used here to calculate the bispectrum was an efficient FFT-based algorithm which enables the calculation of the triple products of the Fourier transforms over *k* non-overlapped segments in which the total signal of acceleration has previously been divided (Sáez et al. 2014b). Symmetry relations in the frequency plane $\{f_1, f_2\}$ resulting from the above definition make that the first quadrant of this plane contains two symmetric regions with respect to the straight line $f_1 = f_2$.

In general, a peak in the bispectrum at the point (f_1, f_2) implies a frequency coupling between the three frequencies f_1, f_2. and $f_1 + f_2 = f_3$. In terms of phase coupling, this peak can only be related with two possible situations, Quadratic Phase Coupling, QPC, or Constant Phase, CP. Only in the first QPC case the energy of the third frequency is provided by the energy of the other two. The values associated to the corresponding phases in both QPC and CP cases are $0/\pm\pi$ rad or a constant value different of the above mentioned, respectively. The study of the biphase is thus critical to elucidate what kind of coupling exists and to do so, a statistical strategy based on the consideration of a global biphase histogram was proposed (Sáez et al 2014b, 2015). Wrapping up, this global histogram is constructed based on the *k* partial histograms associated with the values of the biphases of each one of the different *k* segments considered at the corresponding frequency couplings. If the global histogram has only an absolute maximum, it gives the most probable value of the biphase. On the contrary, if there are more peaks, the relative intensity enables to evaluate the percentage of QPC or CP in the signal (Sáez et al 2014b).

The second magnitude used in the analyses of spectral nonlinearities is the trispectrum (fourth order spectrum). The trispectrum is sensitive to the kurtosis of the signal therefore, it can detect symmetric nonlinearities. From mathematical point of view is defined as,

$$|T_k(f_1, f_2, f_3)| = |X(f_1) \cdot X(f_2) \cdot X(f_3) \cdot X^*(f_1 + f_2 + f_3) \qquad (11)$$

$$\angle T_k(f_1, f_2, f_3) = \theta(f_1) + \theta(f_2) + \theta(f_3) - \theta(f_1 + f_2 + f_3) \qquad (12)$$

where $\mathrm{X}(f_i)$ denotes de Fourier Transform of the acceleration considered at the frequency f_i, X^* its complex conjugate and $\theta(f_i)$ the phase of the Fourier Transform X at a frequency f_i . The subindex k is related, as mentioned before, with the methodology of k non-overlapped segments used for the obtaining of this magnitude. The trispectrum relates three independent frequencies (f_1, f_2, f_3) and it is sensitive to the coupling between them. In the frequency space $\{f_1, f_2, f_3\}$ the principal domain of the discrete trispectrum is composed of two regions, the first one is defined by positives values of frequencies $(f_1 > 0, f_2 > 0, f_3 > 0)$, in which the fourth frequency is equal to the sum of the three frequencies$(f_1 + f_2 + f_3 = f_4)$. The second region, is defined by $(f_1 > 0, f_2 > 0, f_3 < 0)$ and now, the frequency coupling results in a contribution at another frequency f_4 equal to $f_1 + f_2 - f_3 = f_4$. As in the biphase case, the triphase global histogram technique is applied here in order to check when cubic phase coupling (CPC) or constant phase (CP) conditions are accomplished. If the triphase is 0/$\pm\pi$ rad, as we argued before, a cubic phase coupling, CPC is produced. In this case the three frequency components result in an energetic contribution at a frequency equal to their sum. In the other cases, the system is coupled in frequency but not in phase.

Data corresponding to the Progress M-29M (61P Mission) reboosting is used to illustrate these considerations. Due to the fact that this spacecraft used the aft port of the Zvezda module to perform the ISS reboost, calculations were restricted to three acceleration signals in the direction of the disturbance, X_A. Figs. 6 and 7 show the results obtained by using data coming from the JEM/Kibo 121f05 SAMS sensor. Concerning Fig. 6, two bispectrum peaks are detected P1(57,57) and P2(57,114). Taking into account the information contained in the biphase histograms, the first P1 point is associated to a QPC behavior while the second P2 point is associated to a CP behavior. In other words, the power associated to the f_3 is given by the power of f_1 and f_2. Fig. 7 plots the trispectrum of the same signal. Three main peaks are detected at the positions: a) (57,57,57), b) (57,57,-57) and c) (114,57,-57). To check if the points present CPC, Fig. 8 plots the corresponding triphase histograms. Remark, that only the last two points exhibit a cubic phase coupling. This means that only in these cases the power of the fourth frequency is provided by the power of the other three.

It is important to point out that to ensure statistical confidence the maximum segment size to compute the FFT should be the (r-1)th root of the total length when handling the rth order spectrum (r=2 for bispectrum and r=3 for trispectrum). In case of bispectrum the statistical confidence is perfectly accomplished while for trispectrum it needs special conditions, such as long signals, to be achieved. Therefore, in the present case, the investigation of the reboosting period was impossible due to its short duration. No phase coupling during the eight hours analyzed has been observed for low/structural frequencies, which usually are enhanced during the reboosting maneuvers. On the contrary, spectral nonlinearities were detected at high frequencies values. This fact indicates that the origin of these nonlinearities can be provoked by wear parts of mechanical or electrical engines needed to support life and experiments in the Station.

3.- Conclusions

During the last five years a set of digital signal processing techniques have been developed in the aerospace field in order to characterize the vibratory environment of some of the fluid dynamic ESA experiments. These techniques were successfully applied in long thermodiffusion experiments such as the IVIDIL and DCMIX ones and can help the experimentalists to easily detect the possible disturbances that could appear during the runs.

All these implemented tools are an additional contribution to the NASA's conventional techniques in a joint effort to get to know in a more exhaustive way the mechanical behavior of the ISS. The authors expect that these techniques can be used to improve the microgravity quality of new future international space platforms.

References

Cohen, L. : Time-Frequency Analysis: Theory and Applications. Englewood Cliffs, NJ: Prentice-Hall (1995)

Dubert, D., Ollé, J., Jurado, R., Gavaldà, Jna., Laverón-Simavilla, A., Ruiz, X., Shevtsova, V.: Characterization of the accelerometric environment of DCMIX2/3 experiments. Microgravity Sci Tec. 30, 683-697 (2018)

Hrovat, K.: Analysis Techniques for Vibratory data, Nasa 7th Annual Microgravity Environment Interpretation Tutorial (MEIT-2004)

https://pims.grc.nasa.gov/html/ISSAccelerationArchive.html. Accessed 31th January 2019 (2019)

Jules, K., McPherson, K., Hrovat, K., Kelly, E., Reckart, T.: A status report on the characterization of the microgravity environment of the International Space Station. Acta Astronaut. 55, 335–364 (2004a)

Jules, K., McPherson, K., Hrovat, K., Kelly, E.: Initial characterization of the microgravity environment of the International Space Station: increments 2 through 4. Acta Astronaut. 55, 855–887 (2004b)

Jules, K., Hrovat, K., Kelly, E., Reckart, T.: International Space Station Increment 6/8 Microgravity Environment Summary Report. NASA Technical Report. NASA/TM-2006-213896 (2006)

Jurado, R., Simón, M.J., Pallarés, J., Gavaldà, Jna., Laverón-Simavilla, A., Ruiz, X., Shevtsova, V.: Some considerations on the vibrational environment of the DSC-DCMIX1 experiment onboard ISS. Acta Astronautic. 129, 345–356 (2016)

Kantz, H., Schreiber, T.: Nonlinear Time Series Analysis; Cambridge University Press (2005)

Kelly, E.: Analysis Techniques for Quasi-Steady Data, Nasa 7th Annual Microgravity Environment Interpretation Tutorial (MEIT-2004)

Marín-Genescà, M., Dubert, D., Simón, M.J., Ollé, J., Gavaldà, Jna., Ruiz, X.: ISS Quasi-Steady accelerometric data as a tool for the detection of external disturbances during the period 2009-2016. Microgravity Sci Tech. 30(5), 611-634 (2018)

McPherson, K., Hrovat, K., Kelly, E., Keller, J.: A researcher's guide to the International Space Station Acceleration Environment. NASA Report NP-2015-11-040-JSC (2015).

Mialdun, A., Legros, J. -C., Yasnou, V., Sechenyh, V., Shevtsova V.: Contribution to the benchmark for ternary mixtures: Measurement of the Soret, diffusion and thermodiffusion coefficients in the ternary mixture THN/IBB/nC_{12} with 0.8/0.1/0.1 mass fractions in ground and orbital laboratories. Eur. Phys. J. E 38**,** 27 (2015)

Ollé, J., Dubert, D., Gavaldà, Jna., Laverón-Simavilla, A., Ruiz, X., Shevtsova, V.: Onsite vibrational characterization of DCMIX2/3 experiments. Acta Astronautic. 140, 409–419 (2017)

Rogers, M., Hrovat, K., Kelly, E., Reckart, T.: Accelerometer data analysis and presentation techniques. NASA Lewis Research Center, Cleveland (1997)

Sáez, N., Gavaldà, Jna., Ruiz, X., Shevtsova, V.: On the vibrational environment of the "Influence of Vibrations of Diffusion of Liquids" experiment; Proceedings of the 11th International Conference on Vibration Problems. Z. Dimitrovovà et al (Eds). Lisboa, Portugal. ISBN 978-989-96264-4-7 (2013)

Sáez, N., Ruiz, X., Gavaldà, Jna., Pallares, J., Shevtsova, V.: Comparative ISS accelerometric analyses. Acta Astronautic. 94, 681 – 689 (2014a)

Sáez, N., Gavaldà, Jna., Ruiz, X., Shevtsova, V.: *Detecting accelerometric* nonlinearities. Acta Astronautic. 103, 16-25 (2014b)

Sáez, N., Ruiz, X., Gavaldà, Jna., Shevtsova, V.: Comparative Analyses of ESA, NASA and JAXA signals of acceleration during the SODI-IVIDIL experiment. Microgravity Sci Tech. 26, 57–64 (2014c)

Sáez, N., Gavaldà, Jna., Ruiz, X., Shevtsova, V.: Nonlinear mechanical onboard the International Space Station: the IVIDIL experiment. I J Space S E. International Journal of Space Science and Engineering 3, 1-15 (2015)

Shanon, C.E.: A Mathematical Theory of Communication. The Bell System Technical Journal, XXVII 379-423 (1948)

Shevtsova, V.: IVIDIL experiment on-board the ISS. Adv Space Res. 46, 672-679 (2010)

Shevtsova, V., Santos, C., Sechenyh, V., Legros, J. -C., Mialdun, A.: Diffusion and Soret in Ternary Mixtures. Preparation of the DCMIX2 Experiment on the ISS. Microgravity Sci Tech. 25(5), 275-283 (2014)

Triller, T., Bataller, H., Bou-Ali, M. M., Braibanti, M., Croccolo, F., Ezquerro, J. M., Galand, Q., Gavaldà, Jna., Lapeira, E., Laverón-Simavilla, A., Lyubimova, T., Mialdun, A., Ortiz de Zárate, J. M., Rodríıguez, J., Ruiz, X., Ryzhkov, I. I., Shevtsova, V., Van Vaerenbergh, S., Köhler, W.: Thermodiffusion in ternary mixtures of water/ethanol/triethylene glycol: first report on the DCMIX3-experiments performed on the International Space Station. Microgravity Sci. Tec 30 (3), 295-308 (2018).

Table 1: Standard and complementary techniques used in the characterization of one or more acceleration signals.

One acceleration signal		
	Time domain	Frequency domain

Standard techniques (NASA)	Raw data Interval averaged (AVG) Interval Root-Mean-Square (RMS) Interval Minum/Maximum (MIN/MAX) Trimmed Mean Filter (TMF)	Fourier Filtering Power Spectral Density (Schuster/Welch periodogram) Short Time Fourier Transform (STFT); Spectrogram Root-Mean-Square (based on Parseval’s theorem) - Cumulative - vs 1/3 octave frequency bands
Complementary tools	Time Entropy (TEN)	Wavelet denoising Thomson periodogram Spectral Entropy (SEN) Frequency Factor Index (FFI) RMS Warning map High Order Spectral Analysis (HOSA); Bi-/Tri-Spectra
More than one acceleration signal		
Standard techniques (NASA)	2D Scatterplot 3D Scatterplot (2D projection)	---
Complementary tools	3D Scatterplot Pearson/Spearman correlation Cross-correlation; cross-correlogram	Cross-spectrogram Coherence (magnitude and relative phase)

Figure captions

Fig.1 Minute by minute evolution of: the relative time entropy, TEN_r (a1, b1 and c1), skewness (a2,b2 and c2) and kurtosis (a3,b3 and c3) of signals coming from

USLab/Destiny (a), Columbus (b) and JEM/KIBO (c) modules. Signals correspond to berthing episode in Z_A direction.

Fig.2 SEN evolution (right side) and the corresponding spectrograms (left side) of the docking episode of signals coming from USLab/Destiny (a), Columbus (b) and JEM/KIBO (c) modules. Signals correspond to docking episode in X_A direction.

Fig.3 SEN evolution (right side) and the corresponding spectrograms (left side) of the docking episode of signals coming from USLab/Destiny (a), Columbus (b) and JEM/KIBO (c) modules. Signals correspond to reboosting episode in X_A direction.

Fig.4 a) RMS a_x acceleration vs. one-third octave frequency bands calculated in the minute 240, b) warning maps. Signals, coming from USLab/Destiny (a1, b1), Columbus (a2, b2) and JEM/KIBO (a3, b3) correspond to docking episode in X_A direction.

Fig.5 a) RMS a_x acceleration vs. one-third octave frequency bands calculated in the minute 240, b) warning maps. Signals, coming from USLab/Destiny (a1, b1), Columbus (a2, b2) and JEM/KIBO (a3, b3) correspond to reboosting episode in X_A direction.

Fig.6 Bispectrum and phase histograms of the signal coming from JEM/KIBO module and corresponding to reboosting episode in X_A direction.

Fig.7 Trispectrum of the signal coming from JEM/KIBO module and corresponding to reboosting episode in X_A direction.

Fig.8 Phase histograms of the main peaks a, b and c of Fig.7.

Abstract

The accelerometric environment of IVIDIL and DCMIX experiments was successively monitored not only to identify the main disturbances that could affect the experiments but as well to ensure the correct interpretation of the experimental results. To do so, the conventional techniques used by NASA have been complemented by new tools developed and adapted to help the surveillance of the runs. A summary of these main new techniques is presented further. To show the potentiality of all these techniques, moderate and strong disturbance episodes such as berthings, dockings and reboostings were analyzed by using acceleration signals that come from three different sensors located in the US Lab. Destiny, Columbus and JEM/Kibo modules, respectively. The first technique proposed is based on the Shannon entropy concept in both time (TEN) and frequency (SEN) domains. It has been found, that SEN technique is a fast and easy tool to detect the different disturbances registered throughout the experiments. The second technique suggested by the authors is based on the RMS values integrated over each one of the one-third octave frequency bands and is called RMS warning map. It is a visual tool which was demonstrated to be very efficient in detecting the range of the frequencies that surpasses the ISS limits requirements, especially when a sudden disturbance occurs. Finally, in order to identify nonlinearities in the frequency domain within a signal, bispectrum and trispectrum functions have been applied. Quadratic and cubic phase couplings have been detected with these techniques only between high frequencies and especially for the signal from JEM/Kibo module.

Fig 1

Click here to access/download;line figure;Fig1.bmp

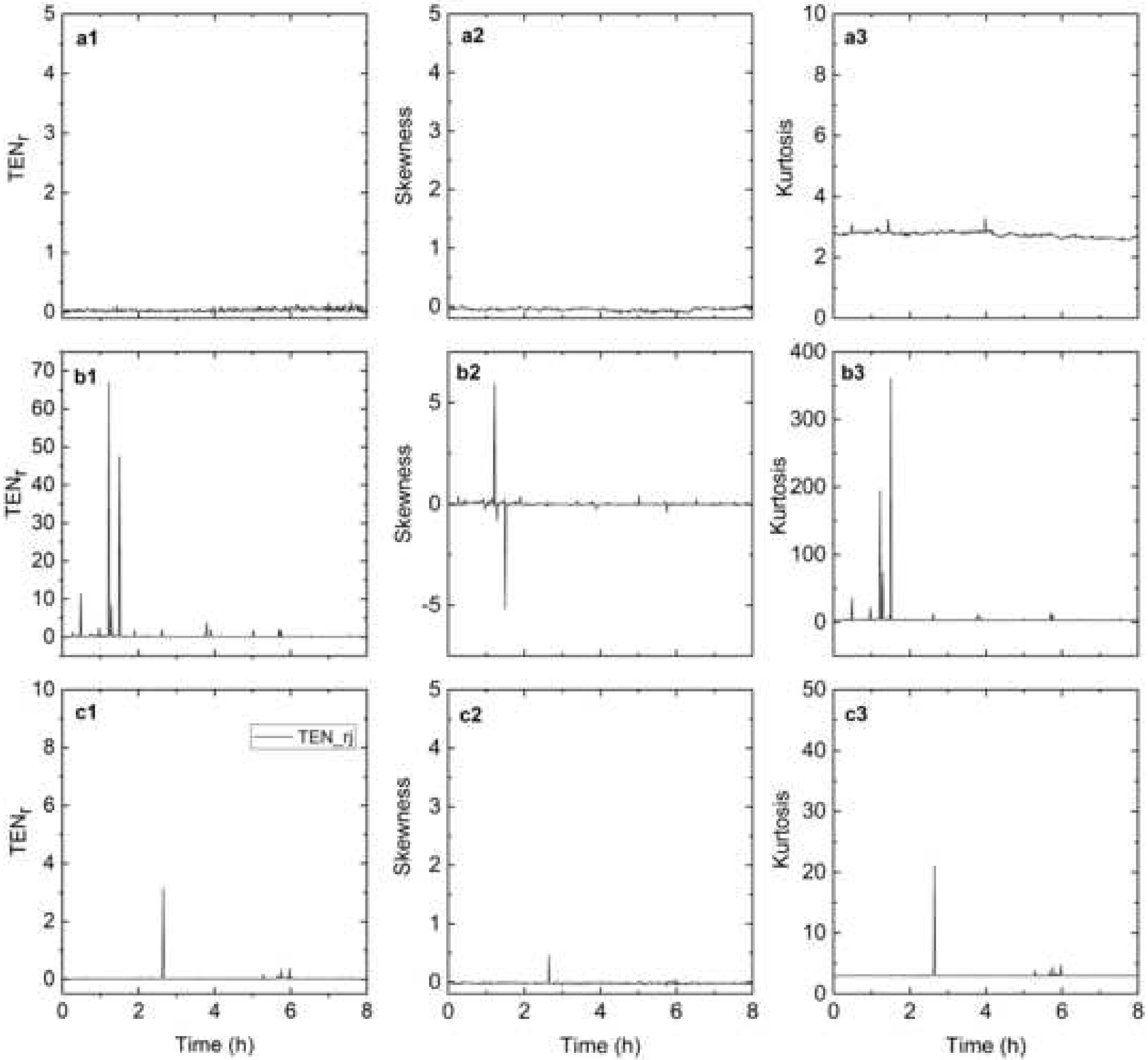

Fig 2

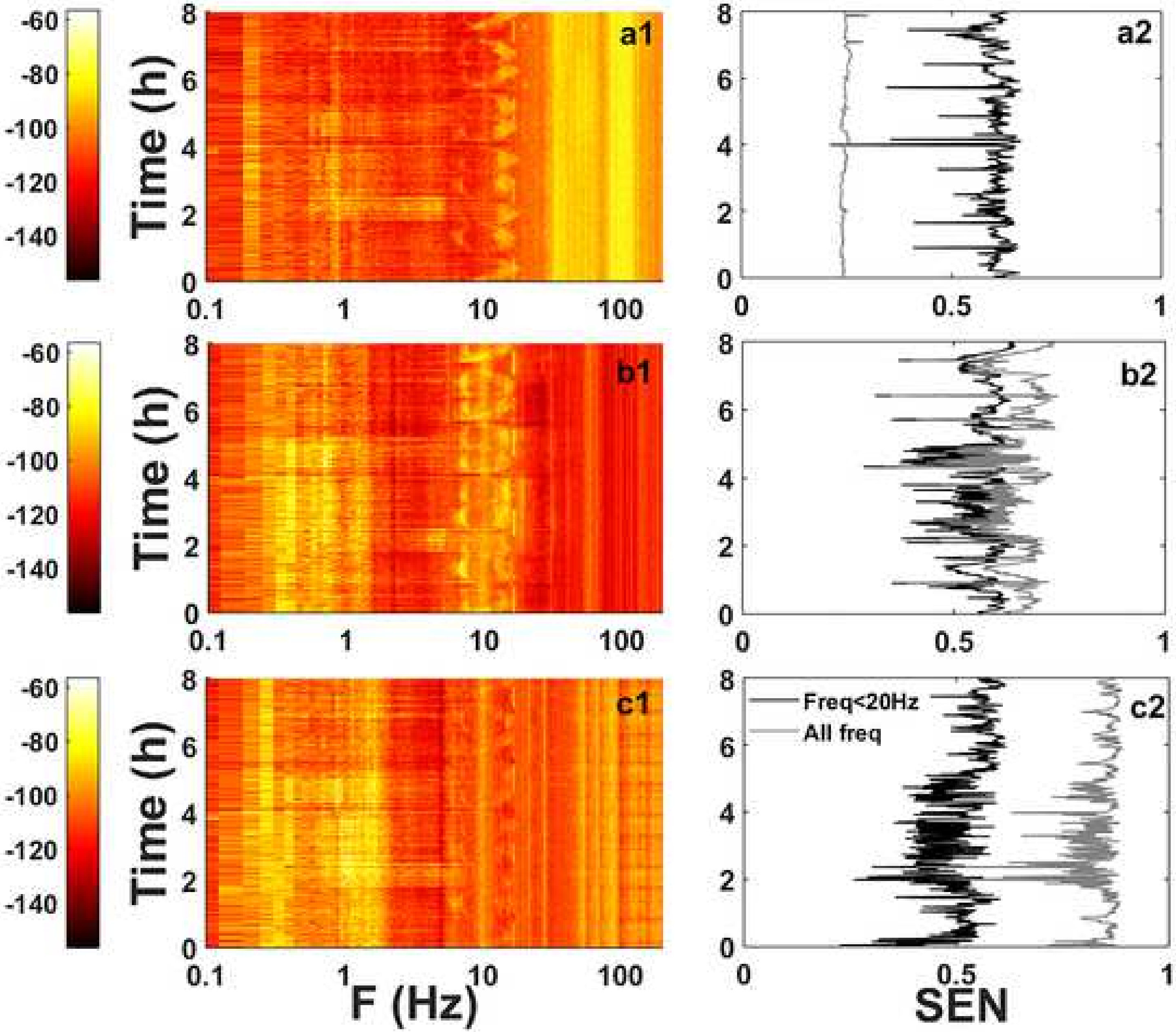

-60
-80
-100
-120
-140
Time (h)
F (Hz)
0.1
1
10
100
a1
b1
c1
a2
b2
c2
SEN
0
0.5
1
Freq<20Hz
All freq

Fig 3

Click here to access/download;colour figure;Fig3.bmp

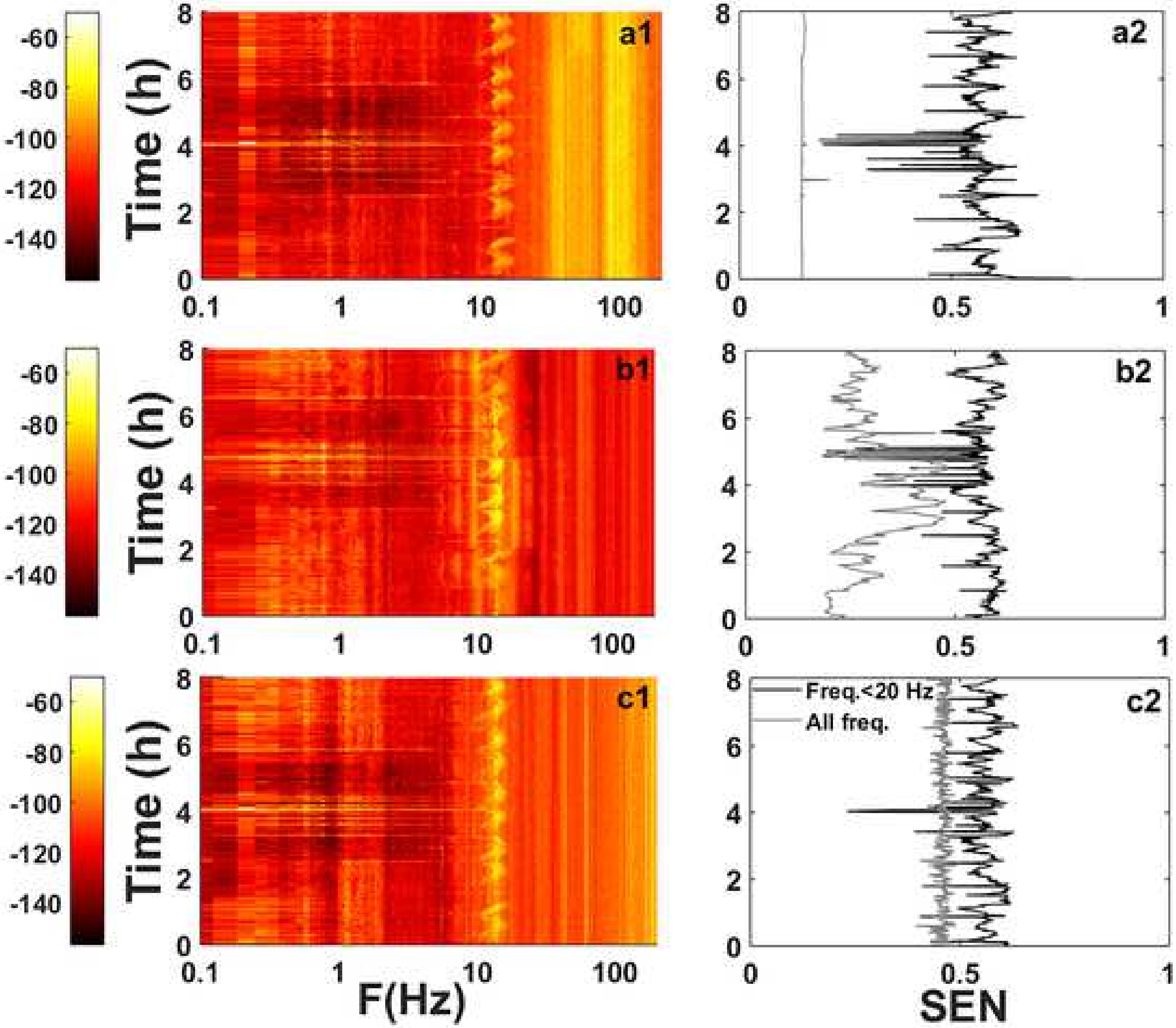

Fig 4

Click here to access/download;line figure;Fig4.bmp

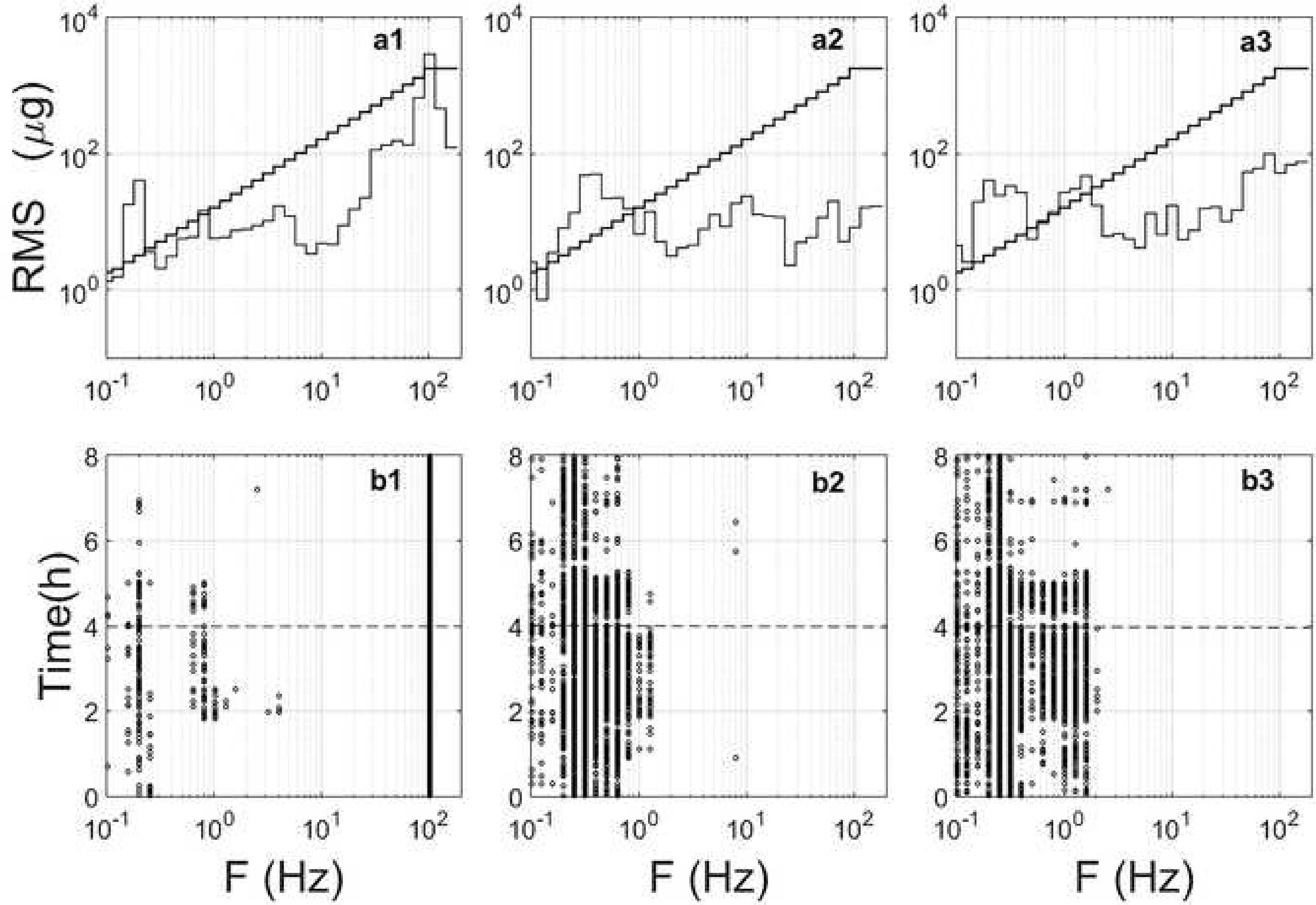

Fig 5

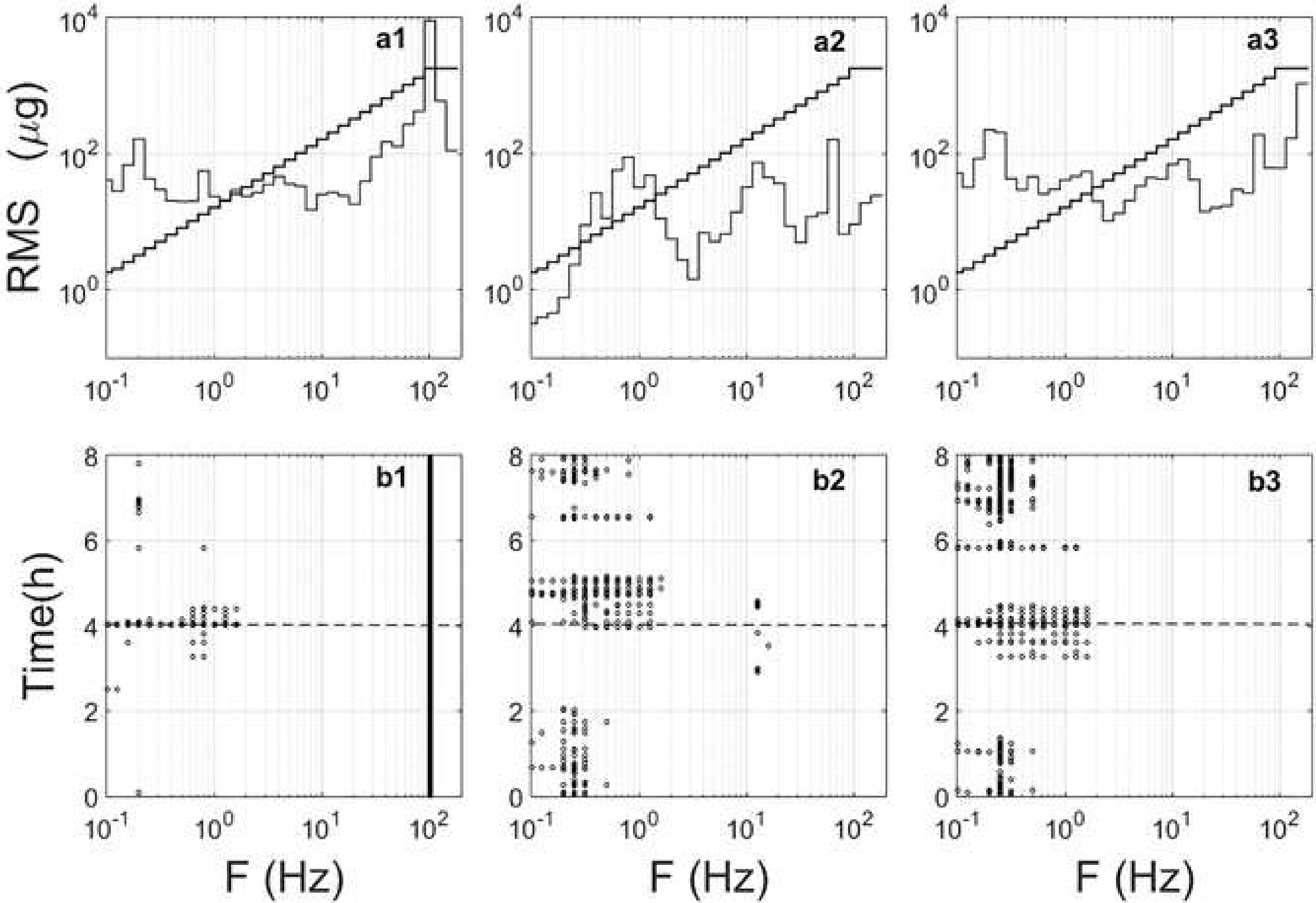

Fig 6

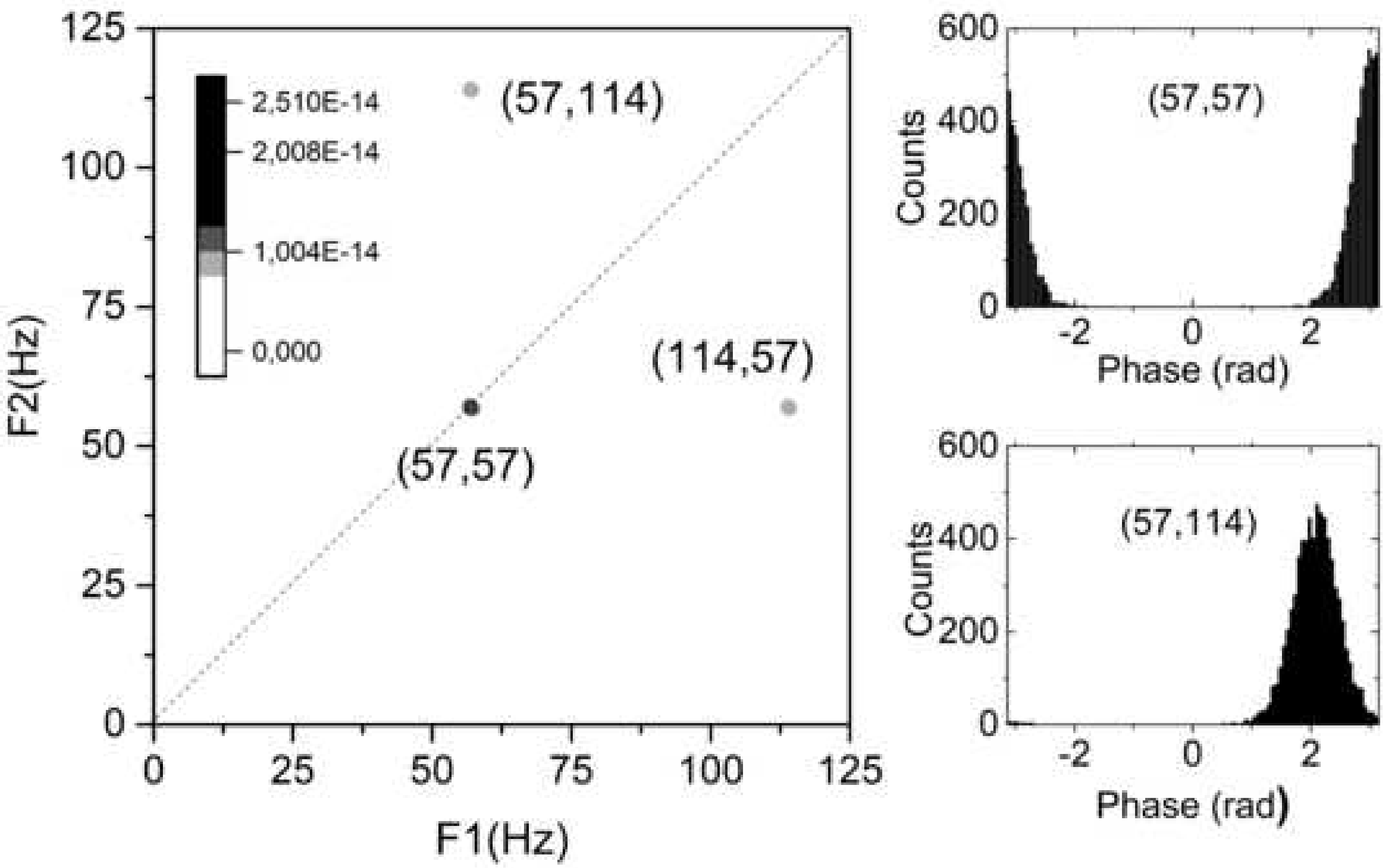
125
100
75
50
25
0
F2(Hz)
2,510E-14
2,008E-14
1,004E-14
0,000
(57,114)
(114,57)
(57,57)
0
25
50
75
100
125
F1(Hz)
600
400
200
0
Counts
(57,57)
-2
0
2
Phase (rad)
600
400
200
0
Counts
(57,114)
-2
0
2
Phase (rad)

Fig 7

Click here to access/download;line figure;Fig7.bmp

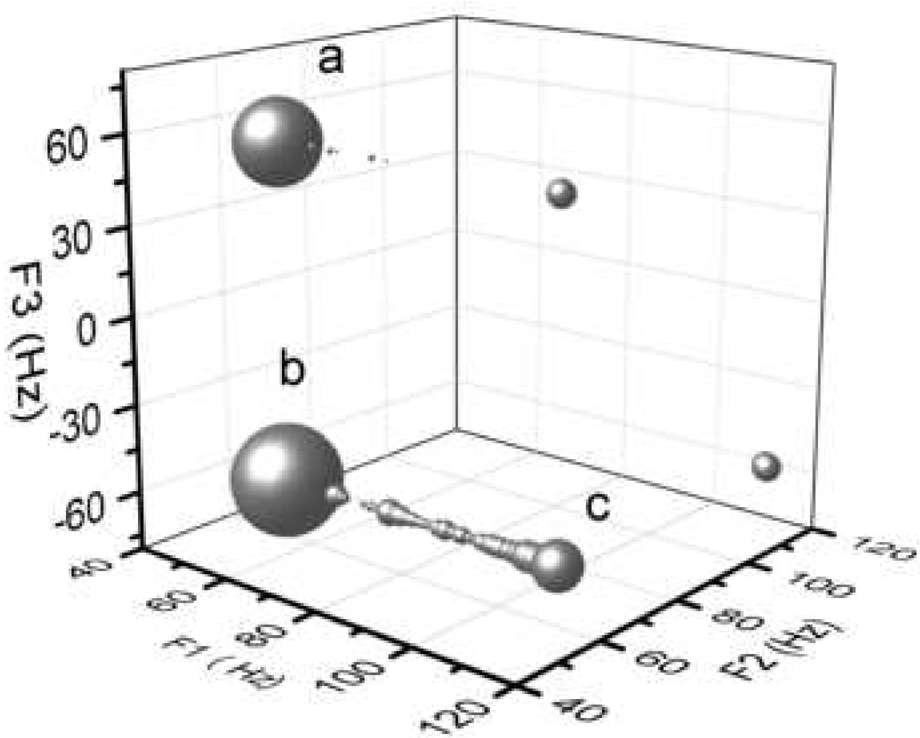

Fig 8

Click here to access/download;line figure;Fig8.bmp